HHS Public Access

Author manuscript

Nat Chem Biol. Author manuscript; available in PMC 2019 July 21.

Published in final edited form as:

Nat Chem Biol. 2019 March ; 15(3): 269–275. doi:10.1038/s41589-018-0209-y.

Junction resolving enzymes use multivalency to keep the Holliday junction dynamic

Ruobo Zhou[1,2,*], **Olivia Yang**[3], **Anne-Cécile Déclais**[4], **Hyeonseok Jin**[5], **Gwang Hyeon Gwon**[5], **Alasdair D. J. Freeman**[4], **Yunje Cho**[5], **David M. J. Lilley**[4], and **Taekjip Ha**[1,3,6,7,8,*]

[1]Department of Physics and Center for the Physics of Living Cells, University of Illinois at Urbana-Champaign, IL, USA

[2]Department of Chemistry and Chemical Biology, Harvard University, Cambridge, MA, USA

[3]Department of Biophysics and Biophysical Chemistry, Baltimore, MD, USA

[4]Cancer Research UK Nucleic Acid Structure Research Group, School of Life Sciences, The University of Dundee, Dundee, U.K.

[5]Department of Life Science, Pohang University of Science and Technology, Pohang, South Korea

[6]Howard Hughes Medical Institute, Baltimore, MD, USA

[7]Department of Biophysics, Johns Hopkins University, Baltimore, MD, USA

[8]Department of Biomedical Engineering, Johns Hopkins University, Baltimore, MD, USA

Abstract

Holliday junction (HJ) resolution by its resolving enzymes is essential for chromosome segregation and recombination-mediated DNA repair. HJs undergo two types of structural dynamics that determine the outcome of recombination: conformer exchange between two isoforms and branch migration. However, it is unknown how the preferred branch-point and conformer are achieved between enzyme binding and HJ resolution given the extensive binding interactions seen in static crystal structures. Single molecule fluorescence resonance energy transfer analysis of resolving-enzymes from bacteriophages (T7 endonuclease I), bacteria (RuvC), fungi (GEN1) and humans (hMus81-Eme1) showed that both types of HJ dynamics still occur after enzyme binding. These dimeric enzymes use their multivalent interactions to achieve this, going through a partially-dissociated intermediate in which the HJ undergoes nearly unencumbered dynamics. This evolutionarily conserved property of HJ resolving-enzymes provides previously unappreciated insight on how junction resolution, conformer exchange and branch migration may be coordinated.

*Correspondence should be addressed to T.H. (tjha@jhu.edu) or R.Z. (ruobozhou@fas.harvard.edu).

Author contributions. R.Z. and T.H. conceived and designed the study. R.Z. and O.Y. performed experiments and analyzed the data. A.-C.D., A.D.J.F. and D.M.J.L. expressed and purified wild type Endo I proteins, Endo I mutants, and GEN1 proteins. A.-C.D. performed Endo I gel retardation assays. H.J., G.H.G. and Y.C. expressed and purified hMus81-Eme1 proteins. R.Z. and T.H. wrote the manuscript with input from the other authors.

Competing financial interests. The authors declare no competing financial interests.

Introduction

Holliday junctions (HJs) are structural intermediates in homologous recombination, a ubiquitous DNA metabolic process that is essential both for DNA repair and genetic variation in all forms of life[1,2]. Once the HJ is formed by the exchange of DNA strands, branch migration extends the heteroduplex, followed by resolution into two duplex DNA molecules by junction resolving enzymes, a group of structure-specific endonucleases[3–5]. A deficiency in junction resolution leads to impaired DNA replication and repair, chromosome instability and dysfunctional mitoses[6].

HJs are highly dynamic DNA structures: the branch point of a junction can migrate spontaneously or through the catalytic function of branch migration enzymes[7,8]; at a given branch point, HJs also undergo spontaneous conformer exchange between two structural isoforms[9–11]. Both types of dynamics influence the outcome of HJ resolution. Branch migration extends or shortens the length of DNA heteroduplex and hence determines the length of gene conversion. The two structural isoforms, or conformers, are correlated with the two alternative orientations of HJ cleavage, which dictate whether the HJ resolution results in gene conversion events either with (cross-overs) or without (non-cross-overs) the exchange of flanking parental DNA sequences. However, it is puzzling how the required branch point and isoform are chosen for HJ cleavage because binding of a resolving enzyme to a junction as seen in their static crystal structures[4,12–16] would not allow conformer exchange or branch migration, and it is unclear whether there is coordination between HJ resolution and these HJ dynamics.

In this work, we use single molecule Fluorescence Resonance Energy Transfer (smFRET)[17] to investigate the HJ dynamics upon binding of a resolving enzyme from diverse organisms, including bacteriophages, bacteria, fungi and humans. We show that initial binding of a resolving enzyme captures the instantaneous structural conformer and branch point at the moment of binding. The resolving enzyme binding does not prevent conformer exchange nor branch migration, and these dimeric enzymes use their multivalency[18] to achieve a short-lived partially dissociated intermediate where the HJ can undergo nearly unencumbered dynamics.

Results

Endo I permits conformer exchange of Holliday junction

In the absence of added divalent metal ions, HJs adopt a 4-fold symmetric square structure (open state **O**; Fig. 1a)[19]. In the presence of Mg^{2+}, HJs fold into two alternatively stacked conformers [19] (**U1** and **U2**; here '**U**' stands for 'unbound' as opposed to '**B**' for protein 'bound'). A single HJ can undergo conformer exchange between **U1** and **U2** and the exchange rate decreases with increased Mg^{2+} concentration[9–11]. The **O** state, although too short-lived to be detected directly in Mg^{2+}, is considered to be a shared intermediate for both conformer exchange and branch migration[8].

To study resolving enzyme binding to HJ using smFRET, we first used Junction 7 (J7)[9–11], the sequence of which does not allow branch migration (Fig. 1a). We attached Cy3 (donor)

and Cy5 (acceptor) to the ends of two adjacent arms such that conformer exchange can be detected as two-state fluctuation in FRET efficiency (E_{FRET}) [2,9,11]. To prevent junction cleavage, we replaced Mg^{2+} with Ca^{2+}. J7 exhibited similar dynamic properties in Ca^{2+} (Fig. 1b) to those in Mg^{2+} [9–11]. The open state **O** of HJ in EDTA maintained a steady E_{FRET} of 0.3. With 10 mM Ca^{2+}, we observed exchanges between **U1** (E_{FRET} = 0.15) and **U2** (E_{FRET} = 0.6) with rates $k_{\mathbf{U1}\rightarrow\mathbf{U2}}$ = 2.1 ± 0.2 s^{-1} and $k_{\mathbf{U2}\rightarrow\mathbf{U1}}$ = 3.5 ± 0.3 s^{-1}.

We first studied endonuclease I from bacteriophage T7[12,14,20–22] (termed 'Endo I' here) (Fig. 1a and Supplementary Fig. 1a). Endo I cleaved surface-immobilized HJs in Mg^{2+} but not in Ca^{2+} (Supplementary Fig. 1b, c), confirming that the enzyme is active under our experimental conditions. In general, the junction resolving enzymes bind in dimeric form with high affinity (K_d ~ 1 nM)[4]. Endo I binding induces either of the two alternative complexes (termed **B1** and **B2**) that differ in coaxial pairing of arms[12,14]. After incubating 10 nM Endo I with surface-immobilized J7 in Ca^{2+}, we flushed out the unbound proteins so that all subsequently observed dynamics can be attributed to the pre-formed complex rather than protein dissociation and binding (Supplementary Fig. 1a; referred to as "flush condition"). The resulting E_{FRET} histogram determined from ~10,000 molecules contained two peaks at E_{FRET} = 0.15 and 0.35, assigned to **B1** and **B2**, respectively, based on structural considerations [12,14] (Fig. 1c). In the flush condition, most molecules were bound with proteins, as is evident by the nearly complete disappearance of **U2** population. The smFRET-time traces showed slow exchanges between **B1** and **B2** (Fig. 1d) at rates $k_{\mathbf{B1}\rightarrow\mathbf{B2}}$ = (1.1 ± 0.4)×10^{-4} s^{-1} and $k_{\mathbf{B2}\rightarrow\mathbf{B1}}$ = (1.0 ± 0.4)×10^{-4} s^{-1}. Interestingly, ~30 % of such transitions showed a short-lived intermediate (Fig. 1d and Supplementary Fig. 2) which we will discuss in the next section.

After observing the complexes in Ca^{2+}, we flushed the sample chamber with buffer containing EDTA. A broad peak was observed in the E_{FRET} histogram (Fig. 1c), and correlation analysis[23] revealed that the time traces contained anti-correlated fluctuations of donor and acceptor intensities (I_D and I_A) with the time scale of 0.11 ± 0.02 s (Supplementary Fig. 3), likely due to fast exchange between **B1** and **B2** previously hypothesized to occur in EDTA[14]. When Ca^{2+} buffer was reintroduced, the relative populations of **B1** and **B2** were different from those prior to the EDTA pulse. This redistribution probably occurs because the **U1**/**U2** equilibrium is different from that of **B1**/**B2**. It is likely that the initial Endo I binding captures the **U1**/**U2** equilibrium which only later relaxes to the **B1**/**B2** equilibrium. Indeed, single molecule time traces capturing the moment of Endo I binding showed that for J7 molecules that were locked into **B2**, 93% had been in **U2** ($E_{0.6}$), and only 7% had started from **U1** ($E_{0.15}$) (Fig. 1e and Supplementary Fig. 4a).

Population redistribution after EDTA pulse was also observed (Supplementary Fig. 5) for three mutants of Endo I[12,20,24]: 1) EndoΔ, lacking the 16 amino-acids N-terminal tail and possessing slower HJ cleavage, 2) K67A, a catalytically-impaired mutant, and 3) K67AΔ, combining both mutations. All three showed increased exchange rates between **B1** and **B2** (Fig. 1f) with K67AΔ having the highest rate, suggesting that their bound states are less stable than the wild type.

Endo I permits branch migration through an intermediate

To investigate branch migration we used two previously described HJ constructs [7]: J5m contains a central 5-bp homologous sequence so it can migrate over six branch points, and J0m is an otherwise identical junction that lacks homology so its branch point cannot migrate (Fig. 2a). We attached the fluorophores to the diametrically-opposed arms so that E_{FRET} is sensitive to the branch point movement but not to conformer exchange (Fig. 2a and Supplementary Fig.6). Any E_{FRET} dynamics seen in J5m but not in J0m can be attributed to branch migration. smFRET data for J0m by itself confirmed that labeling configuration is insensitive to conformer exchange because **O**, **U1** and **U2** merged into one degenerate state (E_{FRET}=0.3 or $E_{0.3}$) (Fig. 2b, c).

Upon Endo I binding, J0m exhibited an $E_{0.45}$ state which represents a degenerate mixture of **B1** and **B2** (Fig. 2c) but also underwent brief excursions to an $E_{0.3}$ state (Fig. 2b; blue-shaded regions). The brief excursions to $E_{0.3}$ are unlikely due to complete dissociation and binding of another Endo I molecule because unbound proteins were washed out. $E_{0.3}$ excursions occurred more frequently with the Endo I mutants (Fig. 2d and Supplementary Fig. 5c, e). Such enhanced transition rates for Endo I mutants were also observed for the **B1↔B2** conformer exchange of Endo I-bound J7 (Fig. 1f) where a short-lived state with a E_{FRET}=0.6 value was often observed as an intermediate (Fig. 1d and Supplementary Fig. 2), indicating this intermediate represents a loosely bound mode. Therefore, we assigned $E_{0.45}$ to the fully bound (**B**) state of J0m and $E_{0.3}$ to a partially-dissociated (**PD**) state through which conformer exchange occurs.

Unlike J0m which showed a constant E_{FRET} value with Ca^{2+}, J5m showed fluctuations in a broad range of 0.1-0.7, likely due to branch migration[7] (Fig. 2e). Upon Endo I binding, the E_{FRET} peak shifted toward higher values while maintaining a broad range of 0.2-0.8, probably reflecting instantaneous branchpoint positions trapped by Endo I binding (Fig. 2c and Supplementary Fig. 4b and 5d). Most time traces (Fig. 2e and Supplementary Fig. 7a, b) comprised constant E_{FRET} values, but with occasional episodes, which we attribute to **PD**, of E_{FRET} fluctuations similar to what were observed for bare J5m. Consistent with this assignment, $k_{\mathbf{B}\rightarrow\mathbf{PD}}$ rates were higher for the mutant proteins (Fig. 2d), sharing the trend of $k_{\mathbf{B}\rightarrow\mathbf{PD}}$ observed for enzyme-bound J0m. Similar smFRET time traces containing **PD** could also be observed in Mg^{2+} with the catalytically-impaired Endo I (K67A) (Supplementary Fig. 8). $k_{\mathbf{PD}\rightarrow\mathbf{B}}$ did not change even in the presence of saturating (100 nM) Endo I, further ruling out the possibility that **B↔PD** transitions were due to full dissociation and binding of the enzyme (Supplementary Fig. 7c).

We could directly observe branch migration as an abrupt change between two different steady E_{FRET} values via **PD** (black arrows, Fig. 2e and Supplementary Fig. 7e-g), showing that **PD** is indeed an intermediate for branch migration. An EDTA pulse redistributed the E_{FRET} populations (Fig.2c and Supplementary Fig. 5), suggesting that an Endo I-bound junction can undergo extensive branch migration in EDTA. Endo I-bound J5m could also undergo slow branch migration in Ca^{2+} (Supplementary Fig. 7d).

Taken together, our data suggest the following model. **PD** serves as an intermediate that allows a resolving-enzyme-bound junction to undergo both branch migration and conformer

exchange. Immediately after binding to a HJ, the enzyme fixes the instantaneous branch position and conformer. The equilibrium population distribution for branch position and conformer is different with and without the enzyme, and the enzyme-bound junction approaches the new equilibrium over time. Indeed, we found direct evidence in smFRET time traces that **PD** acts as an intermediate for branch migration (black arrows, Fig. 2e and Supplementary Fig. 7e-g) and conformer exchange (Fig. 1d and Supplementary Fig. 2a).

RuvC permits both types of HJ dynamics through PD

To test whether cellular (i.e. non-phage) HJ resolving enzymes exhibit similar behaviour, we investigated *E. coli* RuvC[25–27]. Unlike Endo I which is in the restriction endonuclease superfamily, RuvC belongs to the integrase superfamily[28]. Junction resolving enzymes of the integrase superfamily exhibit marked sequence specificity for cleavage (Supplementary Fig. 1c) though they can bind equally well to HJs of any sequence[3,29]. RuvC binding induces a 2-fold symmetrical X-shaped HJ structure with two alternative conformers[15,30] (Fig. 3a). Indeed, we observed two populations for RuvC-bound J7 (Fig. 3b; E_{FRET} = 0.15 for **B1** and 0.35 for **B2**) with a strong preference for **B1**. Time traces for RuvC-bound J7 exhibited **B1**↔**B2** exchanges through **PD**. **PD** is relatively long-lived and had imbedded within it rapid exchange between **U1** ($E_{0.15}$) and **U2** ($E_{0.6}$) (Fig. 3c and Supplementary Fig. 9a), with rates similar to those of protein-free J7 (Fig. 3d). Therefore, upon partial dissociation of RuvC, J7 undergoes conformer exchange nearly unencumbered by the still bound RuvC. **PD** was also observed in a flipped experimental scheme where RuvC was immobilized (Supplementary Fig. 9b), and the addition of saturating concentration (500 nM) of RuvC did not significantly change its average lifetime ($\tau_{\mathbf{PD}}$) (Fig. 3e, Supplementary Fig. 9c, d), confirming that **PD** does not represent full dissociation.

The cross-correlation analysis suggests anti-correlated fluctuations between I_A and I_D with two time components 0.15 ± 0.01 and 3.5 ± 0.2 s (Fig. 3e). The faster component is likely related to the conformer exchange of J7 within **PD**, and the slower component to the transitions between **PD** and **B**. From the real time traces, we could also deduce that when RuvC-bound J7 enters and exits a **B** state, it does so while maintaining coaxial partners. For example, 86% of ***PD***→**B2**→***PD*** events occurred as **U2**→**B2**→**U2** (red circles, Fig. 3f).

We further examined the possibility for branch migration proceeding within a RuvC-bound junction. RuvC binding only slightly reduced E_{FRET} for both J5m and J0m (Supplementary Fig. 10), but unlike the control J0m, RuvC-bound J5m exhibited anti-correlated fluctuations between I_A and I_D, with two time components 0.21 ± 0.01 and 4.2 ± 0.1 s (Fig. 3c, e, and Supplementary Fig. 11), consistent with branch migration. The fast component is likely related to the branch migration rate within **PD** and is slightly slower than that obtained from protein-free J5m, indicating that branch migration persists in **PD** but with a slower rate. The slow component is likely due to the **B**↔**PD** transitions, and is indeed similar to the slow component observed in RuvC-bound J7. In addition, because our junctions do not contain the consensus RuvC cleavage sequence, making HJ cleavage in Mg^{2+} inefficient[29,31] (Supplementary Fig. 1c), we could further show that RuvC-bound junction in Mg^{2+} also undergoes conformer exchange and branch migration via **PD** (Supplementary Fig. 9d, e and Supplementary Fig. 11b, c). The observed rates for these processes were 100-fold higher for

RuvC compared to wild type Endo I as a result of more frequent visits to **PD**. The greater tendency to visit **PD** may help RuvC in the search for its consensus cleavage sequence.

Next, we examined the **B↔PD** transitions for a HJ construct containing one RuvC cleavage site 5'-(A/T)TT↓(G/C)-3'[32] and labelled to report on conformer exchange as in J7 (referred to as RCUNC1). RCUNC1 can be cleaved by RuvC, but more slowly than with both cleavage sites as previously reported[32] (Supplementary Figs. 12a, b). At 10 mM Ca^{2+}, RuvC-bound RCUNC1 showed single molecule behaviours similar to those obtained for RuvC-bound J7 (Fig. 3c and Supplementary Fig. 12c, d). Therefore, introducing a cleavage site does not change the overall behaviour except for small differences in the rates of visiting **PD** (Supplementary Fig. 12e).

Increasing ionic strength makes PD more frequent

Because many DNA-protein interactions can be weakened by increases in ionic strength, we investigated the ionic strength dependence of **B↔PD** transitions. For Endo I (K67A)-bound J5m, $k_{\mathbf{B}\rightarrow\mathbf{PD}}$ was at the minimum at 10 mM Ca^{2+}, and increased as [Ca^{2+}] was further increased (Supplementary Fig. 13a). This [Ca^{2+}] dependence is well aligned with the [Ca^{2+}] dependence measured by gel shift assays: in the low concentration range (<1 mM), Ca^{2+} stabilizes the Endo I binding, whereas in the higher concentration range (≥ 10 mM), increasing [Ca^{2+}] decreases the binding stability (Supplementary Fig. 14). Similarly, for RuvC-bound J7, $k_{\mathbf{B1}\rightarrow\mathbf{PD}}$ was at the minimum at 1 mM Ca^{2+}, and increased as [Ca^{2+}] increased above 1 mM (Supplementary Fig. 13b and Supplementary Fig. 9f, g). When [Ca^{2+}] was kept at 10 mM, increasing [NaCl] also increased $k_{\mathbf{B1}\rightarrow\mathbf{PD}}$ (Supplementary Fig. 13c). Overall, **PD** is more frequently visited at increased ionic strengths and therefore should correspond to a binding mode with lower binding stability compared to the **B** states.

GEN1 binding permits conformer exchange

To test if our observations can be generalized to a eukaryotically conserved junction resolving enzyme GEN1[5], we examined GEN1 from a thermophilic fungus. The current structural model of GEN1-bound HJ is that one pair of opposite arms of the HJ are coaxially aligned, while the other pair are rotated toward each other around the axis of the coaxial arms to include an angle of close to 90°[16]. This structural model predicts that **B1** and **B2** would be merged into one degenerate E_{FRET} state when Cy3 and Cy5 are attached to the ends of two adjacent HJ arms, making J7 a suitable HJ construct to monitor the transitions between **B** and **PD**. Because GEN1 binding requires junctions with longer arms[16], we extended the arms of J7 from 11 to 20 bp to create J7E (Fig. 4a and Supplementary Fig. 9h).

At 10 mM Ca^{2+}, the unbound J7E exhibited transitions between **U1** ($E_{0.05}$) and **U2** ($E_{0.4}$) (Supplementary Fig. 15a). GEN1 binding induced a dominant peak at $E_{0.1}$, representing the degenerate mixture of **B1** and **B2** (and **U1**), and a small peak at $E_{0.4}$ (**U2**). Time traces showed that the bound J7E transited from the bound state ($E_{0.1}$) to the **PD** mode exhibiting **U1↔U2** transitions (Fig. 4b), similar to the behaviour of RuvC-bound J7. The **PD** lifetime ($\tau_{\mathbf{PD}}$) was 3.6 ± 0.3 s (Supplementary Fig. 15b) and $k_{\mathbf{B}\rightarrow\mathbf{PD}}$ was 0.034 ± 0.003 s^{-1}, both similar to those observed for RuvC-bound J7. Furthermore, the **U1↔U2** transitions had

similar rates to those obtained with protein-free J7E (Fig. 4c), indicating that the conformer exchange is unencumbered in **PD** of GEN1-bound junction.

hMus81-Eme1 permits conformer exchange and branch migration

We next investigated the human heterodimeric endonuclease hMus81-Eme1. This enzyme acts cooperatively with other endonucleases by preferentially cleaving the junctions that have already been nicked by other endonucleases such as SLX1-SLX4[33–35]. Because hMus81-Eme1 binding also requires junctions with longer arms[36], we used J7E (Fig. 4a). E_{FRET} histograms of hMus81-Eme1-bound J7E (Supplementary Fig. 15c) were similar to those of GEN1-bound J7E (Supplementary Fig. 15a) and RuvC-bound J7 (Fig. 3b). Time traces of unbound J7E exhibited E_{FRET} fluctuations due to conformer exchange, and these fluctuations persisted in hMus81-Eme1 bound complexes (Fig. 4d and Supplementary Fig. 16), indicating that exchange occurs without full protein dissociation. E_{FRET} fluctuations appear to involve more than two states, suggesting the existence of a **PD** intermediate between **B1** and **B2** (Fig. 4d). To test if hMus81-Eme1 binding still allows branch migration, we used J5m and a variant that contains a nick within the homologous region (n-J5m; Fig. 4a and Supplementary Fig. 15d). It has been shown that a nick does not prevent branch migration[37]. hMus81-Eme1 efficiently cleaved n-J5m but not J5m (Supplementary Fig. 1c), consistent with its role in junction resolution after the first unilateral cleavage[33,36]. hMus81-Eme1-bound n-J5m and J5m exhibited E_{FRET} fluctuations with similar rates, but not the control J0m, indicating that hMus81-Eme1 permits branch migration (Fig. 4e and Supplementary Figs. 17 and 18).

Multivalent interactions between junctions and resolving enzymes

Since junctions in **PD** behave like their unbound counterparts in conformer exchange and branch migration, a significant amount of bonds at the DNA-protein interface must be broken. Because most resolving enzymes function as dimers, it is possible that one subunit within the dimer, or even more interactions at the binding interface, has been disengaged in **PD**, exposing the protein for competitive binding by additional DNA. Indeed, adding either unlabelled junction or duplex DNA as competitors to RuvC-bound J7 accelerated RuvC dissociation by at least 20-fold. (Supplementary Fig. 19). smFRET-time traces obtained immediately after adding DNA competitors typically exhibited an irreversible transition from the steady **B1** state to a mode with rapid **U1↔U2** transitions (Supplementary Fig. 19f). This is consistent with a model in which these molecules transit from the **B** state to the unbound state through **PD**, although it is impossible to identify the exact time point for the transition from **PD** to the unbound state. Junction and duplex DNA were equally competitive for Endo I and for Mus81-Mms4, the budding yeast homolog of hMus81-Eme1[38,39]. Faster dissociation induced by competitor DNA suggests that in **PD** a significant fraction of the interactions between the resolving enzyme and the junction are lost, and the dissociated portion is available to interact with DNA competitors.

Discussion

Our study of four contrasting junction-resolving enzymes from bacteriophage, bacteria, fungi and humans suggests that they share similar properties whereby the dynamic processes

of conformer exchange and branch migration can proceed without full dissociation. This is achieved via an intermediate termed **PD** in which the junction may freely sample **U1**, **U2** and **O** states just like unbound junctions, and which serves as the intermediate for exchange between the **B1** and **B2** complexes, and for branch migration (Fig. 5a). Previous structural analyses could not detect **PD** due to its transient nature, and neither conformer exchange nor branch migration could occur within the constraints of a crystal lattice.

Several biochemical studies have shown that the enzymes facilitating branch migration interact specifically with their cognate resolving enzymes and stimulate their cleavage activity, implying possible coordination between junction branch migration and resolution [26,27,40–43]. The **PD** mode discovered in this study provides a potential molecular mechanism for such coordination of branch migration and resolution. The branch migration enzyme and resolving enzyme bind together to the HJ to form a ternary complex, and the ternary complex formation may lock or bias the HJ in the **PD** mode to allow the branch migration enzyme to actively drive branch migration without full dissociation of the resolving enzyme; once the junction reaches its desired cleavage site, the resolving enzyme switches from the **PD** mode to the fully bound mode to achieve junction resolution (Fig. 5b). A structural model for such a ternary RuvABC-junction complex has been previously hypothesized where the HJ lies sandwiched between RuvA and RuvC, and the RuvA-RuvC-junction complex is flanked on two sides by RuvB[27] although this RuvABC mode of action and its potential conservation in eukaryotes have not been demonstrated.

It should be noted that the rates of dynamics measured *in vitro* for the HJs bound by junction resolving enzymes can be slower than the actual rates *in vivo* as these rates may be affected by multiple factors: 1) The presence of the homologous sequence in the HJ core region could increase the frequency of **PD**. For example, the **B→PD** transition rates of J5m determined for all the four Endo I variants were 3-5 fold higher than those obtained for J0m. 2) Branch migration enzymes apply an active mechanical force (~25 pN for RuvAB[44]) to drive branch migration in one direction, which may significantly increase the tendency of visiting **PD** for the resolving enzyme-bound HJ. 3) The interaction strength between the resolving enzyme and HJ controls the frequency of **PD**, which differs among different resolving enzymes and at different ionic strengths. Both conformer exchange and branch migration for RuvC-bound and GEN1-bound HJs occur much faster than for Endo I-bound HJs. And the dynamics of hMus81-Eme1-bound HJs are even faster. In addition, high ionic strength (Na^+ or divalent ion concentration) could increase the frequency of **PD**.

While the interactions of HJ and resolving enzymes have been extensively described in the literature, our results reveal their dynamic nature. Although their exact binding interface in **PD** awaits further investigation, a significant amount of protein-DNA interactions seen in the ground state of the complex, likely at least one of the two subunits, must have been lost to allow the observed HJ dynamics in **PD** with little to moderate levels of hindrance. Our data may have implications on other DNA-protein interactions that are multivalent and can be broken little by little or one at a time to facilitate the recruitment of other proteins to the same DNA molecule[18].

Online Methods

Statistics and Reproducibility

All the experiments shown in this study were repeated at least three times independently with similar results.

DNA sequences and annealing procedures

DNA sequences for making the DNA constructs used in this study can be found in Supplementary Table 2. DNA oligonucleotides were purchased from Integrated DNA Technologies (Coralville, IA). J7, unlabeled J7 and J7E were annealed by mixing the four strands with the molar ratio 1:1:1:1 (final concentration ~10 μM each) in 10 mM Tris:HCl (pH 8.0) and 50 mM NaCl followed by slow cooling from 90°C to room temperature for ~ 2 hours. J3 was prepared by mixing equimolar amounts of the four component oligonucleotides in PNK buffer (New England Biolabs), labelling them with γ-^{32}P-dATP (Perkin Elmer) and T7 polynucleotide kinase (New England Biolabs) followed by slow cooling from 90°C to room temperature for ~ 2 hours. 22-bp dsDNA was annealed by mixing the two strands with the molar ratio 1:1 (final concentration ~10 μM each) in 10 mM Tris:HCl (pH 8.0) and 50 mM NaCl followed by slow cooling from 90°C to room temperature for ~ 2 hours. J5m, n-J5m and J0m were constructed as previously described [7,37,45]. When J5m undergoes spontaneous branch migration, there are six possible donor-acceptor separations of 10, 12, 14, 16, 18, 20 bp for different branch positions. The donor-acceptor separation for J0m is 16 bp.

Protein expression and purification

Wild-type Endo I and Endo I mutants were expressed and purified as previously described[12,20,24,46]. *E. coli* RuvC was purchased from Abcam (Cambridge, MA). *C. thermophilum* GEN1 was expressed and purified as previously described[16]. Full length human (h)Mus81-Eme1 was expressed and purified as previously described [36]. All protein concentrations cited in the text refer to protein dimers. Purified proteins migrated as a single band on a polyacrylamide gel in the presence of SDS (Supplementary Fig. 20).

Single molecule imaging and data acquisition

All smFRET experiments were performed with a total internal reflection fluorescence (TIRF) microscope [47] at RT (22 ± 1°C) in imaging buffer composed of 20 mM Tris (pH 8.0 for Endo I and RuvC, pH7.5 for hMus81-Eme1 and GEN1), 10 mM NaCl, 0.1 mg/ml BSA, 1 mM DTT, oxygen scavenging system (0.5% wt/vol glucose, 3 mM Trolox, 165 U/ml glucose oxidase band 2170 U/ml catalase), with 5 mM EDTA or the desired concentrations of $CaCl_2$/$MgCl_2$. 5% (vol/vol) glycerol was included in the imaging buffer for hMus81-Eme1 and GEN1 measurements. 50-100 pM of Cy3-Cy5 labeled HJ molecules were immobilized on a quartz slide surface coated with polyethyleneglycol (mPEG-SC, Laysan Bio) in order to eliminate nonspecific surface adsorption of proteins [47,48]. Surface immobilization was mediated by biotin-neutravidin binding between biotinylated HJs, neutravidin (Pierce), and biotinylated polymer (Bio-PEG-SC, Laysan Bio). After incubating HJ resolving enzymes (10 nM Endo I/K67A/EndoΔ/K67AΔ, 50 nM RuvC, 70 nM hMus81-

Eme1, or 100 nM GEN1) with the surface-immobilized HJs for 5 min in imaging buffer containing 1 or 10 mM Ca^{2+}, excess unbound proteins were flushed out of the sample chamber using five chamber volumes of imaging buffer and Cy3/Cy5 intensities from single HJs were recorded using an electron-multiplying CCD camera with time resolution of 0.03 s. These protein concentrations resulted in a bound fraction of almost 100%, and the protein binding was stable for a long period of time (for example, at least 1 hr for Endo I and RuvC) after flushing out the unbound proteins. E_{FRET} histograms were generated by averaging for the time period of 0.15 s from ~10,000 HJ molecules each. smFRET data were excluded only if there was only Cy3 signal and lack of Cy5 signal for that single molecule, or if the intensity-time trace obtained for Cy3 or Cy5 exhibited multiple photo-bleaching steps.

For measuring the cleavage of Holliday junction resolving enzymes under single molecule conditions, 100 pM of Cy3/Cy5-labeled HJ (J5m or n-J5m) were immobilized on the PEG surface. Junction resolving enzymes (10 nM EndoΔ, 50 nM RuvC, or 70 nM hMus81-Eme1) were incubated with the surface-immobilized HJ for 5 min in 1 mM Ca^{2+} and the excess unbound proteins were flushed out using buffer containing 1 mM Ca^{2+}. 1 mM Mg^{2+} was then introduced to the sample chamber to trigger the cleavage reaction at room temperature. For both of the two possible cleavage orientations, the cleavage released the part of HJ that contains Cy3. Therefore, the fraction of uncleaved J5m (or n-J5m) can be monitored by determining the mean Cy3 spot count per imaging area (~ 2,500 μm^2) as a function of reaction time. For RuvC cleavage, RCUNC1 and J7E were also used following the same protocol except that 10 mM instead of 1 mM Mg^{2+} was introduced to the sample chamber to trigger the cleavage reaction and prism holder, and that sample stage, and objective were connected to a Thermo NESLAB RTE-7 circulating bath using custom parts to maintain sample temperature at 37 °C.

For the Ca^{2+}-EDTA-Ca^{2+} buffer exchange experiments, 10 nM of wild type Endo I or Endo I mutant (K67A, EndoΔ, or K67AΔ) was incubated with the surface-immobilized HJs (J7, J0m or J5m) in 10 mM Ca^{2+} for 10 min. The first E_{FRET} histogram was obtained 10 min after flushing out unbound proteins using buffer containing 10 mM Ca^{2+}. The second E_{FRET} histogram was obtained 10 min after the first buffer exchange to buffer containing 5 mM EDTA. Finally, the third E_{FRET} histogram was obtained 5 min after the second buffer exchange to buffer containing 10 mM Ca^{2+}. For the resolving enzyme cleavage assay, imaging buffer containing 1 mM Mg^{2+} was introduced to the sample chamber to trigger the cleavage reaction, after incubating and flushing HJ resolving enzymes in imaging buffer containing 1 mM Ca^{2+}. Mean Cy3 spot count per image (each imaging area is ~2,500 μm^2) was determined from images taken from 5-10 different slide regions at different time points after introducing the Mg^{2+} buffer. For the competition binding assay, unlabeled competitor DNA (J7 or 22-bp DNA duplex) was introduced to the sample chamber, after incubating and flushing RuvC proteins in buffer containing 10 mM Ca^{2+}. E_{FRET} histograms were obtained at different times after introducing competitor DNA.

Transition rate determination

The transition rate from the fully bound (**B**) state to the partially dissociated (**PD**) state, $k_{\mathbf{PD}\rightarrow\mathrm{B}}$, was determined from the single exponential fit to the histogram of the dwell times

of the **PD** state. The reverse transition rate, $k_{\mathbf{B}\rightarrow\mathbf{PD}}$, was defined as the total number of **B→PD** transitions observed, divided by the total time that all the molecules spent in the **B** state. The total time here is the cumulative time not only from those molecules showing the **B→PD** transition, but also from the molecules that did not show such transitions but stayed in the **B** state throughout the observation time window, which is limited by the photobleaching life time of Cy dyes and typically ranges from 20 to 300 s under our experimental conditions. Because the **B→PD** transition occurs with a relatively low frequency, Cy3 or Cy5 can be photobleached before a **B→PD** transition can occur, making it not so meaningful to determine the percentage of molecules showing the **B→PD** transitions. Nonetheless, we determined such percentage values for Endo I-bound HJs, and found that these values vary a lot among the four Endo I variants and also depend on the DNA substrate (J0m or J5m): For J0m, it is 23% for Endo I, 42% for K67A, 45% for EndoΔ, and 91% for K67AΔ; For J5m, it is 51% for Endo I, 90% for K67A, 92% for EndoΔ, and 98% for K67AΔ. It is worth noting that the actual percentages of molecules that have the capability to show **B→PD** transitions are likely much more than those numbers have indicated due to the limited observation time window described above. The transition rates between **U1** and **U2** at 10 mM Ca^{2+} were determined using hidden Markov models as previously described [49]. It is worth noting that when the **U1** or **U2** dwell times are shorter than our experimental time resolution (0.03 s), those dwell times would not show up in the time traces and hence were missed from our analysis. Given that **U1**/**U2** dwell times have a single exponential distribution and the average **U1** (or **U2**) dwell time is ~ 0.4 s, we can further estimate the portion of these undetectable **U1** (or **U2**) dwell times to be ~ 7%. In the time traces showing initial binding of Endo I to J7 which locked the J7 molecules into **B2** (Fig. 1f), we detected that 93% had been in **U2**, and only 7% had started from **U1**. Given that our detection would miss 7% of **U2** dwell times, 93% could actually mean that almost 100% of J7 molecules that got locked in **B2** had been in **U2**.

FRET efficiency calculation.

Apparent FRET efficiency (E_{FRET}) was calculated from the fluorescence intensities of the donor (I_D) and acceptor (I_A) using the formula $E_{FRET} = I_A / (I_A + I_D)$. The background and the cross-talk between the donor and acceptor were considered as previously described [47].

Cross-correlation analysis

The cross-correlation analysis was performed as previously described[23,50]. The cross-correlation functions were calculated between donor and acceptor time traces for each HJ molecule, and all the cross-correlations presented in figures are cross-correlations averaged among >200 HJ molecules. We found the cross-correlations for bare J7, J7E, J5m and n-J5m can be fit to a single exponential function, while those for resolving-enzyme-bound J7, J7E, J5m and n-J5m can be fit to a bi-exponential function, yielding one time component for bare HJs and two time components for resolving-enzyme-bound HJs.

Gel electrophoresis

To detect RuvC cleavage, 10 μl of each cleavage reaction was prepared as a mixture of 10 nM DNA substrate (J7E or RCUNC1), 10 nM RuvC, 50 mM Tris-HCl (pH 8.0), 5 mM

$MgCl_2$, 1 mM DTT, 100 μg/mL BSA. For control experiments, RuvC was not included in the mixture. Samples were incubated at RT or 37 °C for 15 min, then stopped by addition of 2 μl of 5× stop buffer (125 mM EDTA, 2.5% SDS, and 50% glycerol). Samples were then run on 10% polyacrylamide gel in 1× TBE buffer.

To determine the $[Ca^{2+}]$ dependence of Endo I binding to HJ, 0.2 nM 5'-^{32}P-labelled four-way DNA junction J3 was incubated with serial two-fold dilutions of endonuclease I (from 1 μM to 15.3 pM) for 10 min at 22 °C in 20 mM Tris-HCl (pH 8.0), 50 mM NaCl, 0.1 mg/ml BSA and the specified concentration of either EDTA (1 mM) or $CaCl_2$ (0.2, 1, 5, 10, 15 or 20 mM). These samples were then mixed with loading buffer (0.25% bromophenol blue, 0.25% xylene cyanol FF and 2.5% Ficoll type 400), loaded onto 8% polyacrylamide gels and electrophoresed in TB buffer containing the specified concentration of either EDTA or $CaCl_2$. Dried gels were exposed to storage phosphor screens (BAS-IP MP 2040), and quantified using a BAS- 1500 phosphorimager (Fuji) and Image Gauge V4.0 software. Data were analyzed as the fraction of DNA bound (f_{bound}) versus the concentration of protein and were fit to a two-state model:

$$f_{bound} = \frac{K_D + P_0 + D_0 - \sqrt{(K_D + P_0 + D_0)^2 - 4P_0D_0}}{2D_0}$$

where total protein and DNA concentrations are P_0 and D_0 respectively and K_D is the dissociation constant (i.e., the inverse of the binding affinity constant K_A).

Code availability

All custom software and codes are available from T.H. (tjha@jhu.edu) or R.Z. (ruobozhou@fas.harvard.edu) upon request or can be downloaded from the Ha Research Group website at http://ha.med.jhmi.edu/resources/.

Data availability

The data that support the findings of this study are available from T.H. (tjha@jhu.edu) or R.Z. (ruobozhou@fas.harvard.edu) upon reasonable request. A Life Sciences Reporting Summary for this study is available.

Supplementary Material

Refer to Web version on PubMed Central for supplementary material.

Acknowledgements.

We acknowledge Ha lab members for experimental help and discussion. This work was supported by grants from the National Science Foundation (PHY-1430124) and the National Institutes of Health (GM 122569) to T.H., and grants from the Korean government (NRF 2018R1A2A1A190 to Y.C.). R.Z. is a Howard Hughes Medical Institute Fellow of the Life Sciences Research Foundation. T.H. is an employee of the Howard Hughes Medical Institute. Work in the Lilley lab is funded by Cancer Research UK program grant A18604.

References

1. Liu Y & West SC Happy Hollidays: 40th anniversary of the Holliday junction. Nat Rev Mol Cell Biol 5, 937–944 (2004). [PubMed: 15520813]
2. Lilley DM Structures of helical junctions in nucleic acids. Q Rev Biophys 33, 109–159 (2000). [PubMed: 11131562]
3. Lilley DM & White MF The junction-resolving enzymes. Nat Rev Mol Cell Biol 2, 433–443 (2001). [PubMed: 11389467]
4. Declais AC & Lilley DM New insight into the recognition of branched DNA structure by junction-resolving enzymes. Curr Opin Struct Biol 18, 86–95 (2008). [PubMed: 18160275]
5. Wyatt HD & West SC Holliday junction resolvases. Cold Spring Harb Perspect Biol 6, a023192 (2014). [PubMed: 25183833]
6. Sarbajna S & West SC Holliday junction processing enzymes as guardians of genome stability. Trends Biochem Sci 39, 409–419 (2014). [PubMed: 25131815]
7. Karymov M, Daniel D, Sankey OF & Lyubchenko YL Holliday junction dynamics and branch migration: single-molecule analysis. Proc Natl Acad Sci U S A 102, 8186–8191 (2005). [PubMed: 15917329]
8. McKinney SA, Freeman AD, Lilley DM & Ha T Observing spontaneous branch migration of Holliday junctions one step at a time. Proc Natl Acad Sci U S A 102, 5715–5720 (2005). [PubMed: 15824311]
9. McKinney SA, Declais AC, Lilley DMJ & Ha T Structural dynamics of individual Holliday junctions. Nat Struct Biol 10, 93–97 (2003). [PubMed: 12496933]
10. Joo C, McKinney SA, Lilley DMJ & Ha T Exploring rare conformational species and ionic effects in DNA Holliday junctions using single-molecule spectroscopy. Journal of Molecular Biology 341, 739–751 (2004). [PubMed: 15288783]
11. Hohng S et al. Fluorescence-force spectroscopy maps two-dimensional reaction landscape of the holliday junction. Science 318, 279–283 (2007). [PubMed: 17932299]
12. Hadden JM, Declais AC, Carr SB, Lilley DM & Phillips SE The structural basis of Holliday junction resolution by T7 endonuclease I. Nature 449, 621–624 (2007). [PubMed: 17873858]
13. Biertumpfel C, Yang W & Suck D Crystal structure of T4 endonuclease VII resolving a Holliday junction. Nature 449, 616–U614 (2007). [PubMed: 17873859]
14. Declais AC et al. The complex between a four-way DNA junction and T7 endonuclease I. EMBO J 22, 1398–1409 (2003). [PubMed: 12628932]
15. Gorecka KM, Komorowska W & Nowotny M Crystal structure of RuvC resolvase in complex with Holliday junction substrate. Nucleic Acids Res 41, 9945–9955 (2013). [PubMed: 23980027]
16. Liu Y et al. Crystal Structure of a Eukaryotic GEN1 Resolving Enzyme Bound to DNA. Cell Rep 13, 2565–2575 (2015). [PubMed: 26686639]
17. Ha T et al. Probing the interaction between two single molecules: fluorescence resonance energy transfer between a single donor and a single acceptor. Proc Natl Acad Sci U S A 93, 6264–6268 (1996). [PubMed: 8692803]
18. Ha T Single-molecule approaches embrace molecular cohorts. Cell 154, 723–726 (2013). [PubMed: 23953107]
19. Duckett DR et al. The structure of the Holliday junction, and its resolution. Cell 55, 79–89 (1988). [PubMed: 3167979]
20. Declais AC, Hadden J, Phillips SE & Lilley DM The active site of the junction-resolving enzyme T7 endonuclease I. J Mol Biol 307, 1145–1158 (2001). [PubMed: 11286561]
21. Duckett DR, Panis MJ & Lilley DM Binding of the junction-resolving enzyme bacteriophage T7 endonuclease I to DNA: separation of binding and catalysis by mutation. J Mol Biol 246, 95–107 (1995). [PubMed: 7853409]
22. Liu J, Declais AC & Lilley DM Mechanistic aspects of the DNA junction-resolving enzyme T7 endonuclease I. Biochemistry 45, 3934–3942 (2006). [PubMed: 16548520]

23. Kim HD et al. Mg2+-dependent conformational change of RNA studied by fluorescence correlation and FRET on immobilized single molecules. Proc Natl Acad Sci U S A 99, 4284–4289 (2002). [PubMed: 11929999]
24. Freeman AD, Declais AC & Lilley DM The importance of the N-terminus of T7 endonuclease I in the interaction with DNA junctions. J Mol Biol 425, 395–410 (2013). [PubMed: 23207296]
25. Bennett RJ, Dunderdale HJ & West SC Resolution of Holliday junctions by RuvC resolvase: cleavage specificity and DNA distortion. Cell 74, 1021–1031 (1993). [PubMed: 8402879]
26. van Gool AJ, Shah R, Mezard C & West SC Functional interactions between the holliday junction resolvase and the branch migration motor of Escherichia coli. EMBO J 17, 1838–1845 (1998). [PubMed: 9501105]
27. Zerbib D, Mezard C, George H & West SC Coordinated actions of RuvABC in Holliday junction processing. J Mol Biol 281, 621–630 (1998). [PubMed: 9710535]
28. Lilley DM & White MF Resolving the relationships of resolving enzymes. Proc Natl Acad Sci U S A 97, 9351–9353 (2000). [PubMed: 10944205]
29. Fogg JM, Schofield MJ, White MF & Lilley DM Sequence and functional-group specificity for cleavage of DNA junctions by RuvC of Escherichia coli. Biochemistry 38, 11349–11358 (1999). [PubMed: 10471285]
30. Bennett RJ & West SC Structural analysis of the RuvC-Holliday junction complex reveals an unfolded junction. J Mol Biol 252, 213–226 (1995). [PubMed: 7674302]
31. Shah R, Bennett RJ & West SC Genetic recombination in E. coli: RuvC protein cleaves Holliday junctions at resolution hotspots in vitro. Cell 79, 853–864 (1994). [PubMed: 8001122]
32. Fogg JM & Lilley DM Ensuring productive resolution by the junction-resolving enzyme RuvC: large enhancement of the second-strand cleavage rate. Biochemistry 39, 16125–16134 (2000). [PubMed: 11123941]
33. Wyatt HD, Sarbajna S, Matos J & West SC Coordinated Actions of SLX1-SLX4 and MUS81-EME1 for Holliday Junction Resolution in Human Cells. Mol Cell 52, 234–247 (2013). [PubMed: 24076221]
34. Castor D et al. Cooperative Control of Holliday Junction Resolution and DNA Repair by the SLX1 and MUS81-EME1 Nucleases. Mol Cell 52, 221–233 (2013). [PubMed: 24076219]
35. Gwon GH et al. Crystal structures of the structure-selective nuclease Mus81-Eme1 bound to flap DNA substrates. Embo Journal 33, 1061–1072 (2014). [PubMed: 24733841]
36. Chang JH, Kim JJ, Choi JM, Lee JH & Cho Y Crystal structure of the Mus81-Eme1 complex. Genes Dev 22, 1093–1106 (2008). [PubMed: 18413719]
37. Palets D, Lushnikov AY, Karymov MA & Lyubchenko YL Effect of single-strand break on branch migration and folding dynamics of Holliday junctions. Biophys J 99, 1916–1924 (2010). [PubMed: 20858437]
38. Parsons CA & West SC Specificity of binding to four-way junctions in DNA by bacteriophage T7 endonuclease I. Nucleic Acids Res 18, 4377–4384 (1990). [PubMed: 2167465]
39. Gaskell LJ, Osman F, Gilbert RJ & Whitby MC Mus81 cleavage of Holliday junctions: a failsafe for processing meiotic recombination intermediates? EMBO J 26, 1891–1901 (2007). [PubMed: 17363897]
40. Matulova P et al. Cooperativity of Mus81.Mms4 with Rad54 in the resolution of recombination and replication intermediates. J Biol Chem 284, 7733–7745 (2009). [PubMed: 19129197]
41. Mazina OM & Mazin AV Human Rad54 protein stimulates human Mus81-Eme1 endonuclease. Proc Natl Acad Sci U S A 105, 18249–18254 (2008). [PubMed: 19017809]
42. Constantinou A, Davies AA & West SC Branch migration and Holliday junction resolution catalyzed by activities from mammalian cells. Cell 104, 259–268 (2001). [PubMed: 11207366]
43. Zhang R et al. BLM helicase facilitates Mus81 endonuclease activity in human cells. Cancer Res 65, 2526–2531 (2005). [PubMed: 15805243]
44. Amit R, Gileadi O & Stavans J Direct observation of RuvAB-catalyzed branch migration of single Holliday junctions. Proc Natl Acad Sci U S A 101, 11605–11610 (2004). [PubMed: 15292509]

Methods-only References

45. Karymov MA, Bogdanov A & Lyubchenko YL Single molecule fluorescence analysis of branch migration of holliday junctions: effect of DNA sequence. Biophys J 95, 1239–1247 (2008). [PubMed: 18424495]
46. Hadden JM, Convery MA, Declais AC, Lilley DM & Phillips SE Crystal structure of the Holliday junction resolving enzyme T7 endonuclease I. Nat Struct Biol 8, 62–67 (2001). [PubMed: 11135673]
47. Roy R, Hohng S & Ha T A practical guide to single-molecule FRET. Nat Methods 5, 507–516 (2008). [PubMed: 18511918]
48. Ha T et al. Initiation and re-initiation of DNA unwinding by the Escherichia coli Rep helicase. Nature 419, 638–641 (2002). [PubMed: 12374984]
49. McKinney SA, Joo C & Ha T Analysis of single-molecule FRET trajectories using hidden Markov modeling. Biophysical Journal 91, 1941–1951 (2006). [PubMed: 16766620]
50. Zhou R et al. SSB Functions as a Sliding Platform that Migrates on DNA via Reptation (vol 146, pg 222, 2011). Cell 146, 485–485 (2011).

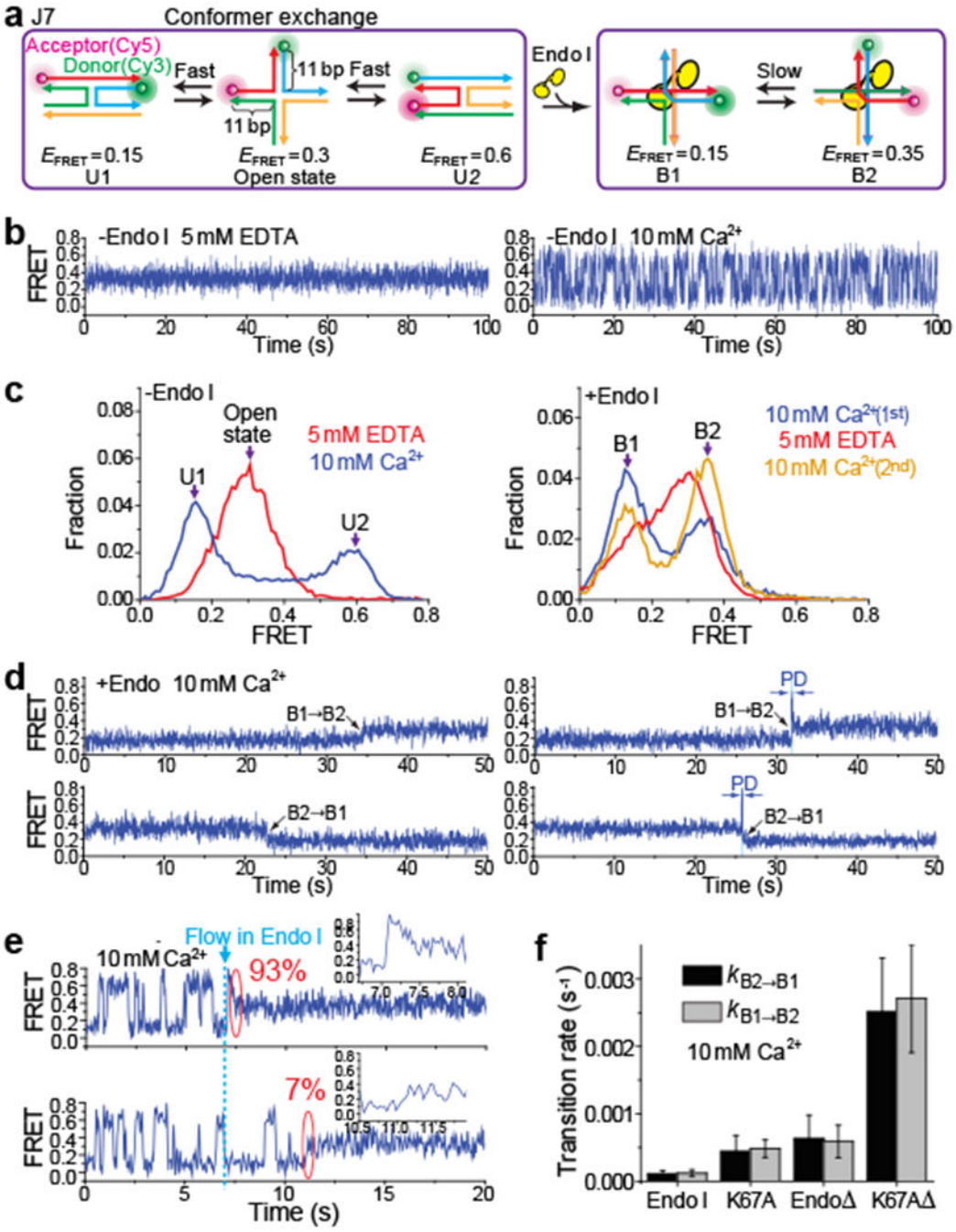

Figure 1: Endo I binding to Holliday junctions captures the instantaneous junction conformer and permits exchange between two isoforms (B1 and B2).

a, Schematic of junction structural dynamics before and after Endo I binding. Junction 7 (J7) comprises four arms of 11 bp. **b,** smFRET-time traces for unbound J7 obtained at 0 or 10 mM Ca^{2+}. **c,** E_{FRET} histograms of unbound J7 at 0 or 10 mM Ca^{2+} (left) and of Endo I-bound J7 obtained in the Ca^{2+}-EDTA-Ca^{2+} buffer exchange experiments (right). **d,** smFRET-time traces of Endo I-bound J7 at 10 mM Ca^{2+}, showing the transitions between **B1** and **B2**. Partial dissociation (**PD**) was observed as an intermediate (blue-shaded region)

for ~30% of the transitions between **B1** and **B2** (right). **e,** Single molecule time traces of J7 showing an Endo I binding event. The blue dashed line indicates the time when 10 nM Endo I were added. The percentages were analyzed from 1,000 HJ molecules. **f,** Conformer exchange rates $k_{B1\rightarrow B2}$ and $k_{B2\rightarrow B1}$ for the four variants of Endo I obtained at 10 mM Ca^{2+}. Data are means ± s.e.m of n = 1,000 HJ molecules. Error bars represent bootstrap estimates of s.e.m..

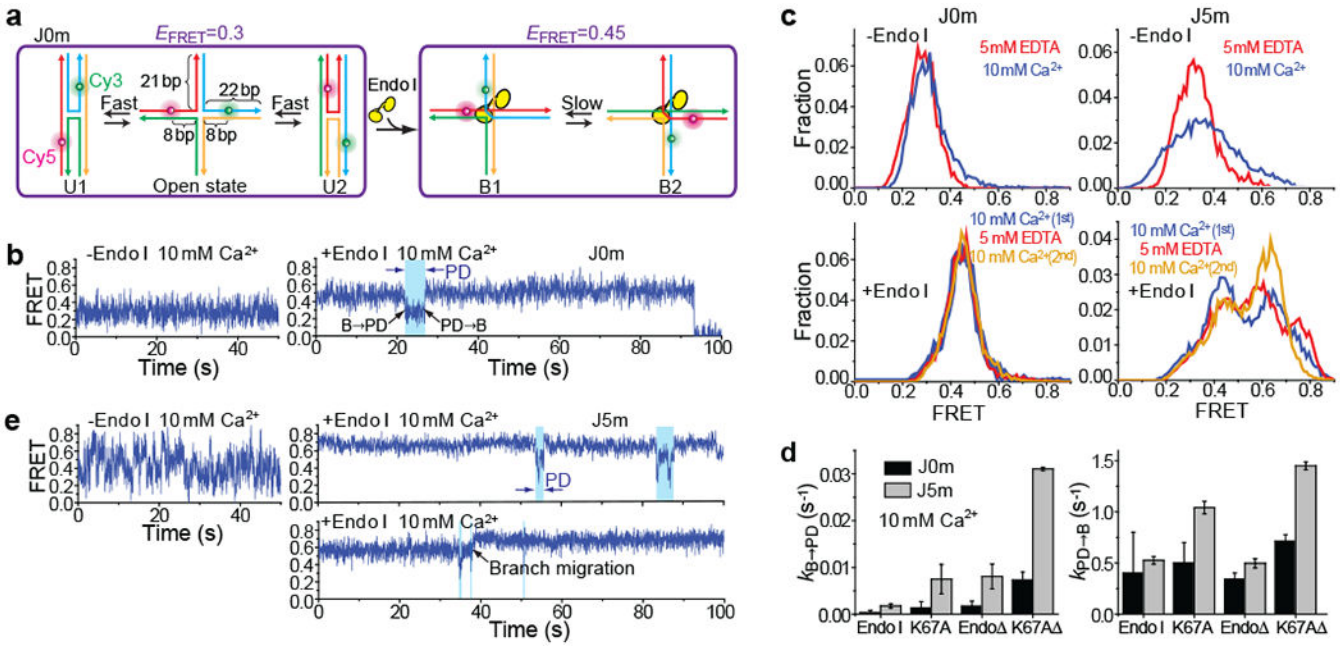

Figure 2: Endo I binding captures the instantaneous branch position and permits branch migration through a partially dissociated intermediate.

a, Schematic of J0m exhibiting different E_{FRET} states before and after Endo I binding. **b,** smFRET-time traces of unbound and Endo I-bound J0m in 10 mM Ca^{2+}. Partial dissociation (**PD**) of Endo I was observed as transient reduction in E_{FRET} (blue-shaded region). **c,** smFRET histograms of unbound J0m or J5m obtained at 0 or 10 mM Ca^{2+} (top), and of Endo I-bound J0m or J5m obtained in the Ca^{2+}-EDTA-Ca^{2+} buffer exchange experiments (bottom). **d,** $k_{B\rightarrow PD}$ and $k_{PD\rightarrow B}$ for four variants of Endo I obtained at 10 mM Ca^{2+}. Data are means ± s.e.m. of n = 1,000 HJ molecules. Error bars represent bootstrap estimates of s.e.m.. **e,** smFRET-time traces of unbound and Endo I-bound J5m in 10 mM Ca^{2+}. Visits to **PD** were observed as transient reduction in E_{FRET} (blue-shaded regions). A representative branch migration event is marked (black arrow).

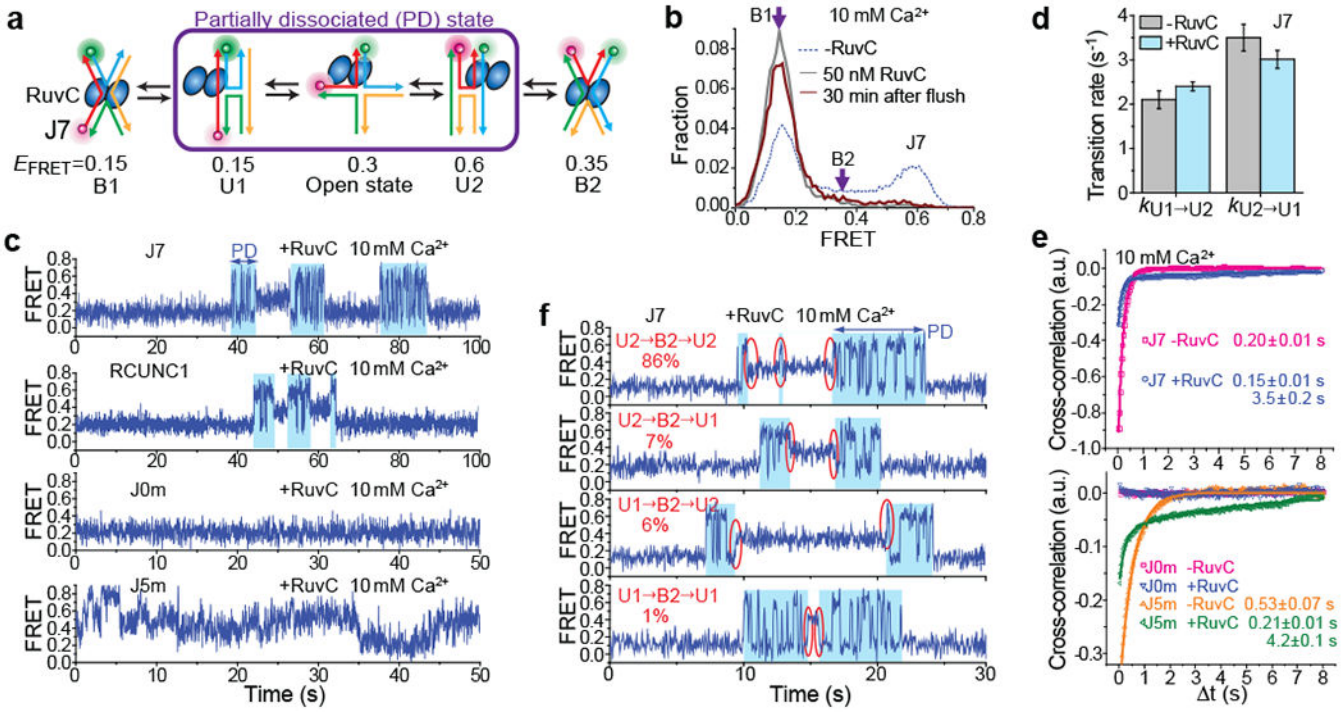

Figure 3: RuvC binding permits conformer exchange and branch migration through PD.

a, Schematic of HJ structural dynamics for RuvC-bound J7. **b,** E_{FRET} histograms of J7, with and without RuvC bound, at 10 mM Ca^{2+}. **c,** smFRET-time traces of RuvC-bound J7, RCUNC1, J0m and J5m at 10 mM Ca^{2+}. Partial dissociation of RuvC was observed as an intermediate (blue-shaded region) between **B1** and **B2**. **d,** The conformer exchange rates between **U1** and **U2** for bare J7 and for RuvC-bound J7 within **PD**. Data are means ± s.e.m. of n = 1,000 HJ molecules. Error bars represent bootstrap estimates of s.e.m.. **e,** Cross-correlations of I_D and I_A for J7E, J0m, J5m and n-J5m, with and without RuvC bound, are fit to single (for free HJs) or double (for RuvC-bound HJs) exponential functions (see also Supplementary Table 1). Means ± s.e.m are indicated (n = 1,000 HJ molecules). **f,** smFRET-time traces of RuvC-bound J7 with different types of **PD→ B2→ PD** transitions. 86% of **PD→ B2→ PD** events occur as **U2→ B2→ U2** (red circles). The percentages were analyzed from 1,000 HJ molecules.

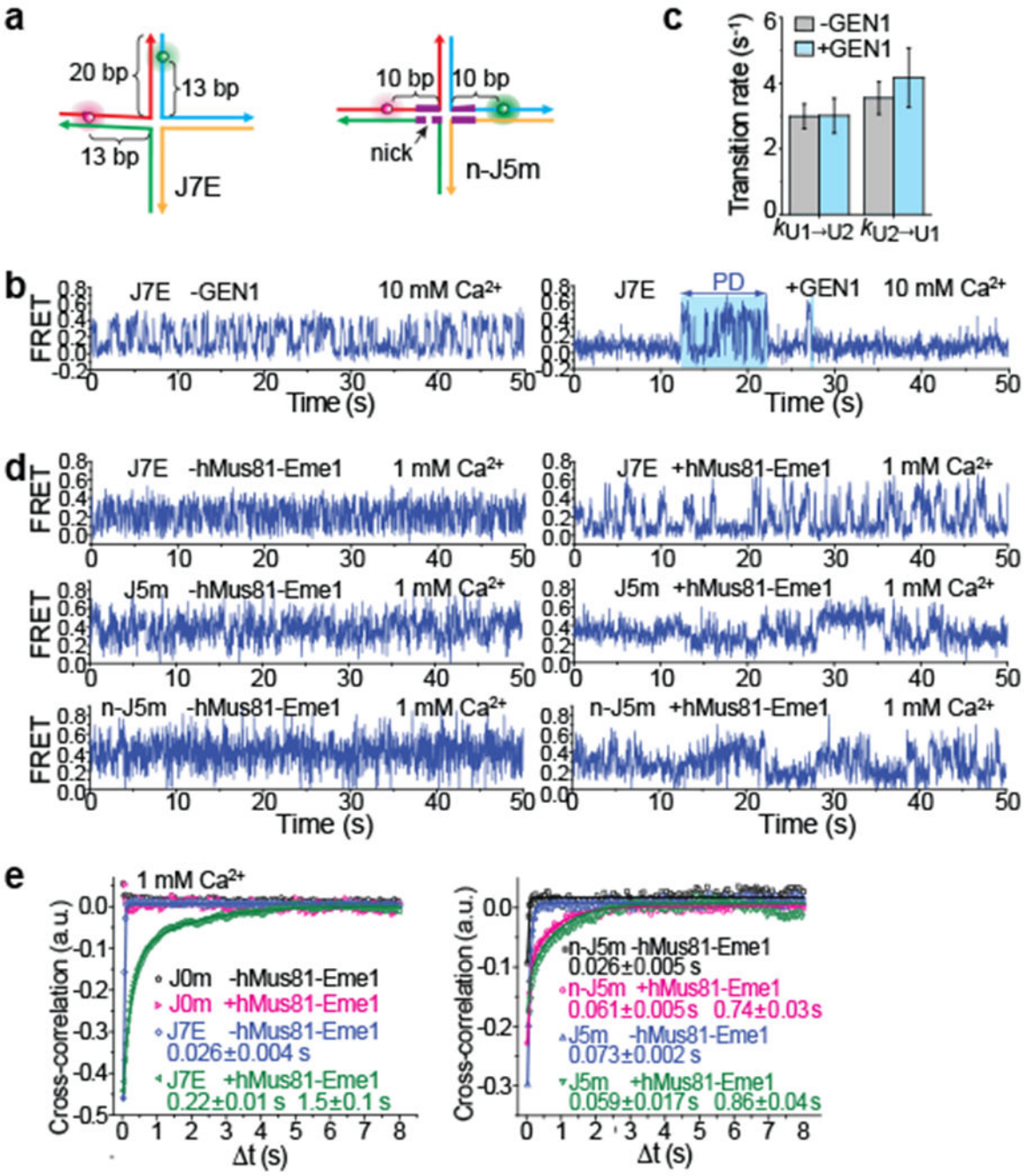

Figure 4: GEN1 and hMus81-Eme1 binding both permit conformer exchange and hMus81-Eme1 binding also permits branch migration.

a, Schematics of J7E and n-J5m. **b,** smFRET- time traces of unbound and GEN1-bound J7E at 10 mM Ca^{2+}. **c,** The conformer exchange rates between **U1** and **U2** for bare J7 and for GEN1-bound J7 within **PD**. Data are means ± s.e.m. of $n = 1{,}000$ HJ molecules. Error bars represent bootstrap estimates of s.e.m. **d,** smFRET-time traces of bare or hMus81-Eme1-bound J7E, J5m and n-J5m at 1 mM Ca^{2+}. **e,** Cross-correlations of I_D and I_A for J7E, J0m, J5m and n-J5m, with and without hMus81-Eme1 bound, were fitted to single (for unbound

HJs) or double (for hMus81-Eme1-bound HJs) exponential functions (see also Supplementary Table 1). Means ± s.e.m are indicated (n = 1,000 HJ molecules).

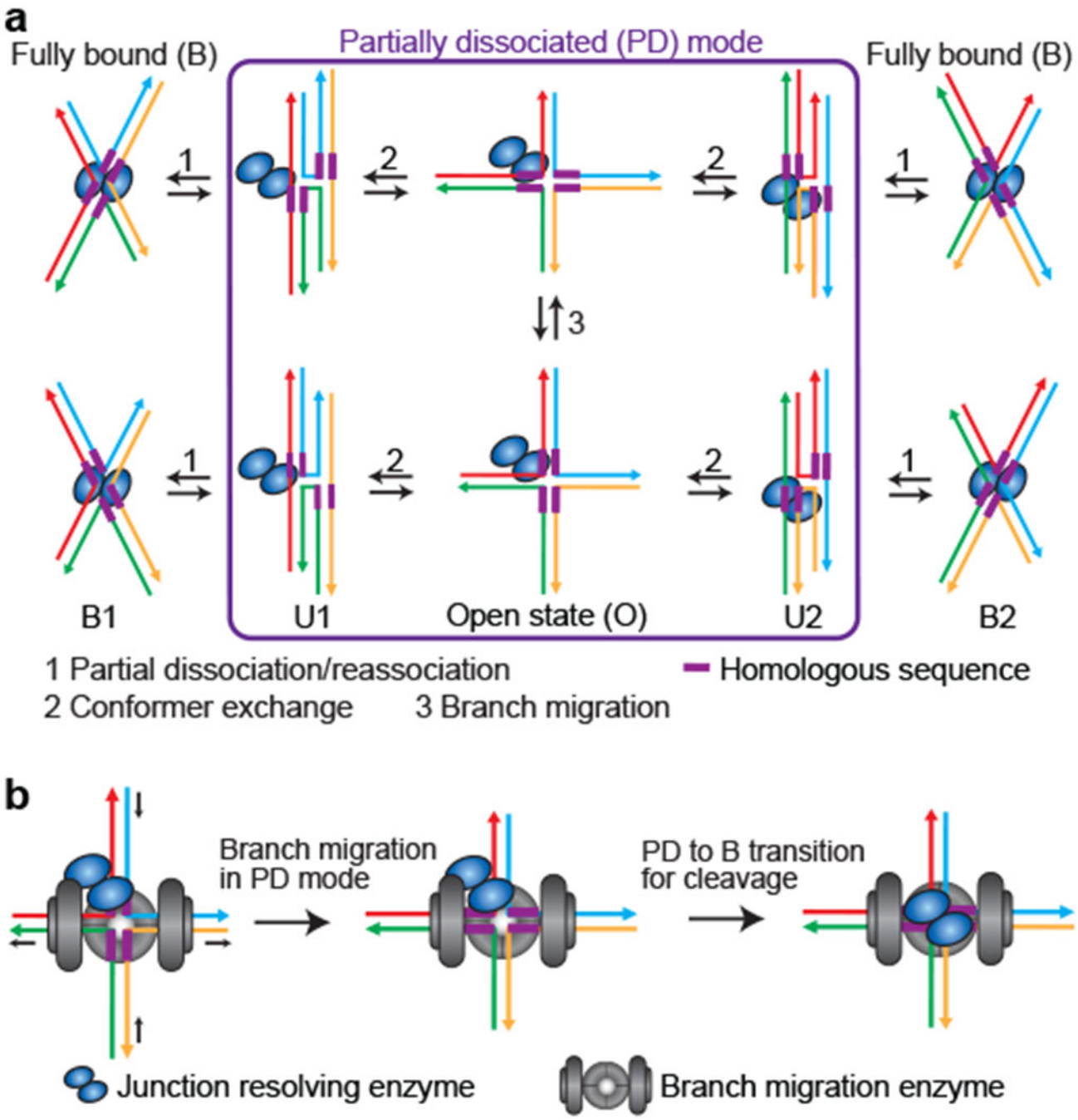

Figure 5: Proposed models for the coordination of junction resolution, conformer exchange and branch migration.

a, Schematic of a kinetic model deduced to describe the dynamics of resolving-enzyme-bound HJs**. PD** serves as an intermediate that allows a resolving-enzyme-bound junction to undergo both branch migration and conformer exchange. **b,** Schematic of the speculative ternary complex containing the branch migration-facilitating enzyme, the junction resolving enzyme and Holliday junction for the coordination of branch migration and junction resolution.